Cutting speed and behaviors of ice using Yb-doped fiber laser

Merlin L. MAH,[1] Andrei V. KURBATOV,[2] Joseph J. TALGHADER[1]

[1] *Dept. of Electrical & Computer Engineering, University of Minnesota, Minneapolis, MN, USA*
[2] *Climate Change Institute and School of Earth & Climate Sciences, University of Maine, Orono, ME, USA*
Correspondence: Joey Talghader, joey@umn.edu
200 Union St SE, Minneapolis, MN 55455

ABSTRACT. The use of a laser to cut or drill ice has been proposed and demonstrated multiple times in previous decades as a novel, but never adopted, machining tool in glaciology and paleoclimate studies. However, with the rapid development of high power fiber-laser technology over the past few decades, it is timely to perform further studies using this new tool. An investigation is made herein on the cutting of ice using a Yb-doped fiber laser emitting at a wavelength of 1070 nm**, the most extensively developed and highest power fiber laser technology, in pulsed and continuous-wave operation. Visible-light observations of clear tap water ice samples, moving at a constant velocity relative to a pulsed laser beam, demonstrate a linear relationship between the duration of a millisecond-range laser pulse and the depth of the meltwater-free cut formed in response. Thermal imaging of the irradiated face shows that peripheral heating trends linearly for pulse lengths greater than 5** ms**. A comparison of pulse trains with a constant time-averaged power suggests that shorter pulses are advantageous in slot-cutting efficiency and in minimizing visible alterations in the surrounding ice. These results demonstrate the viability of powerful fiber-compatible lasers as a tool for ice sample retrieval and processing.**

Keywords: *Ice, Laser, Cutting, Sampling, Temperature*

This version accepted 24 September 2024 for publication as:

Mah M.L., Kurbatov A.V., and Talghader J.J. (2024) Cutting speed and behaviors of ice using Yb-doped fiber laser. *Cold Regions Science and Technology* **228**, 104335 (doi: 10.1016/j.coldregions.2024.104335)

INTRODUCTION

Intermediate or deep sampling of ice from Earth's polar sheets is currently conducted exclusively by mechanical or thermal (heated annulus) core drilling. (Davidge et al., 2022) Drilling from the surface to the bedrock or depths of interest produces a fairly complete continuous archive, but also represents an enormous logistical undertaking in remote and inhospitable field sites. Certain scientific applications require additional ice volume from selected depths, whether to capture sparsely distributed biosignatures located by downhole spectrography (Eshelman et al., 2019) or to supplement a break from fractured ice core (Gow and Meese, 2007) (Ahn et al., 2004). The Deep Ice-Sheet Coring (DISC) drill was capable of drilling replicate core deviating from an existing borehole, as successfully performed on the newly-drilled WAIS Divide borehole in austral 2012–2013, but required 59 metric tons of deployed equipment and has not to date been used again. (Slawny et al., 2014) Even contemporary fast-access technologies (Goodge and Severinghaus, 2016) cannot fulfill small ice sample requisitions without a substantial cost and logistics footprint.

Near-infrared fiber lasers could serve as a transformative cutting tool to fulfill existing needs in both field sample retrieval and laboratory processing. In the field, a borehole tool directing a beam carried by optical fiber from the surface could excise new ice volumes with a lightweight logistics footprint; in the lab, brittle ice samples could be precisely partitioned without vibration-heavy mechanical bandsaws. Before any specific laser-based tools can be detailed, it must be experimentally demonstrated that such a laser can expediently make cuts in ice, that the potential of trapped meltwater refreezing is either not an issue or can be effectively addressed, and that this process can take place without thermally compromising the scientific value of the surrounding ice.

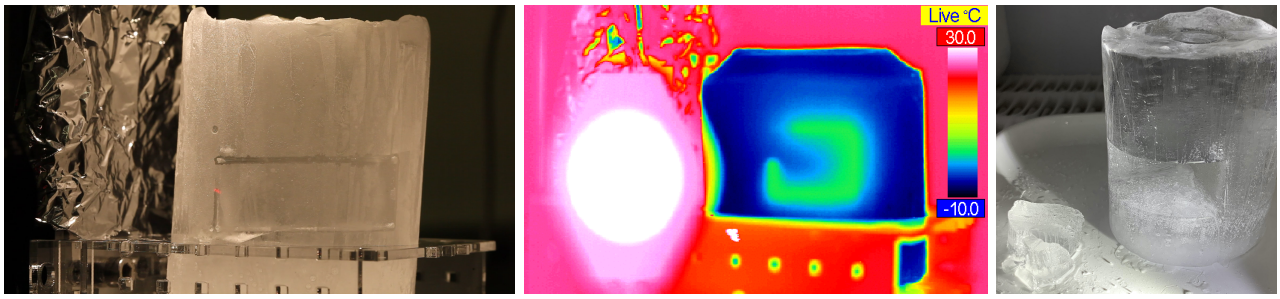

(a) Cut path (b) Thermal video (c) Wedge

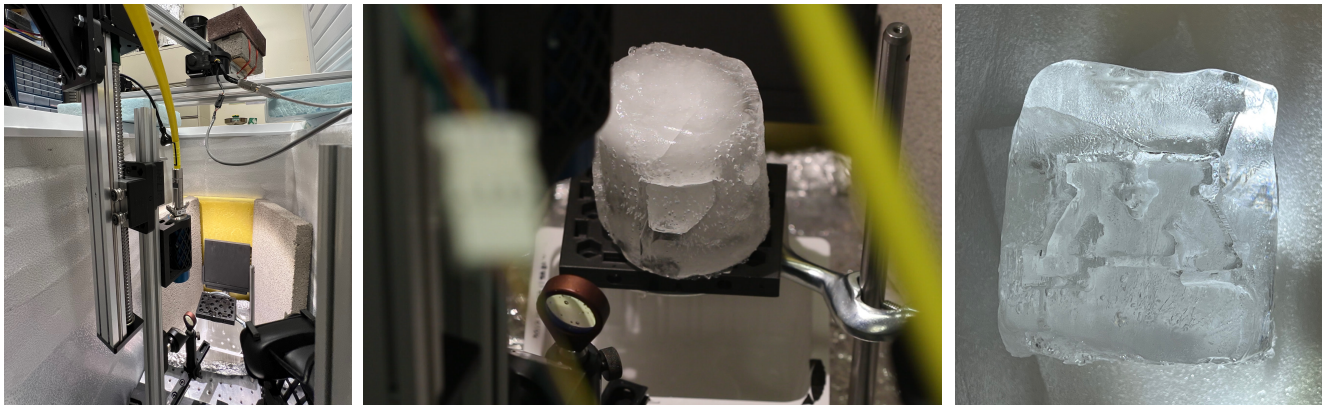

(d) Fiber-based setup (e) Wedge in progress (f) UMN logo

Fig. 1: Qualitative experiments demonstrating the laser excision from an ice body of a self-terminating wedge. (a) A Nd:YAG laser, emitting 1064 nm light at 80 W CW, traces a rectangular path approximately 20 mm high and 90° in arc on the surface of a 75 mm diameter tap water ice cylinder. (A low-power red laser indicates where the near-infrared cutting beam is aimed.) The ice sample sits in an aluminum foil-backed acrylic holder on a vertical translation stage which is in turn mounted on a rotation stage, allowing the fixed focus point of the stationary laser beam to be maneuvered along the cylinder surface. The setup is at room temperature but the ice is introduced at -20 °C, causing condensation to rapidly form. (b) Thermal imaging of a similar trial shows a large region of significant surface heating surrounding the laser cut path. (c) The ice cylinder and excised wedge, returned to a -24 °C freezer. (d) The delivery fiber of a Yb-doped fiber laser is attached to the carriage of a vertical translation stage, which is mounted via a fixed-length arm on a motorized rotation stage, and lowered into an open-top laboratory chest freezer. (e) A wedge ∼30 mm high by 20° in arc is defined on a 5 cm diameter cylinder. The bottom right corner of the otherwise rectangular profile is truncated due to the stages being inadvertently choreographed to move at the same time; when done intentionally, this can (f) be used to cut decidedly non-rectilinear samples, such as this University of Minnesota logo.

Prior art

Laser machining in ice core research has generally been limited to applications such as ablation for inductively-coupled plasma mass spectrometry (ICP-MS). (Sneed et al., 2015) (Müller et al., 2011) (Lunga et al., 2014) (Bohleber et al., 2020) (Peensoo, 2021) These scenarios usually use ultraviolet or infrared short-pulse lasers to controllably liberate small volumes of material for analysis. Limiting energy delivery to ps or fs pulses, shorter than the time scale for slower thermal processes such as conduction, can transition the ice directly from solid to vapor or plasma phases in order to avoid any possible alteration or movement of chemical, isotopic, or trapped gas contents. This makes short- and ultrashort- pulse lasers scientifically and technically attractive for cutting and sampling applications. Unfortunately, cutting speed considerations stipulate that any laser cutting system produce a high average power, and existing short pulse laser systems with this characteristic are frequently quite costly. (Chichkov et al., 1996) (Cheng et al., 2013)

For a more immediately affordable tool to machine ice at a rapid rate, we turn to continuous-wave or "quasi-CW" millisecond-regime pulsed lasers. Such sources, with output powers of hundreds or thousands of watts, have over the past few decades supplanted mechanical cutting in a variety of industry scenarios. A handful of beachheads were also attempted in cryospheric science. Long-wavelength infrared (LWIR) lasers were investigated for use to assist icebreakers through sea ice. (Clark et al., 1973) Zeller, Dreschhoff, and Laird described a working prototype of an ice coring drill which used an orbiting laser beam instead of a mechanical drill head, although development did not seem to have been pursued further. (Zeller et al., 1991) More recently, Sakurai et al. measured the rates of laser hole drilling in a block of ice. (Sakurai et al., 2016) While many of these works speculated on potential advantages at shorter wavelengths, all eventually relied on CO_2 laser sources, which

emit 10.6 µm light from a gas-filled glass tube. The average power of a CO_2 laser can be scaled to tens of kilowatts (with commensurate increases in system size) and the long wavelength has an absorption length in ice of less than 0.1 mm, which is in theory desirable as the energy will interact with a smaller volume of ice. (Warren, 2019) However, this gas laser technology requires a bulky pressurized tube and an RF power supply sufficient to initiate plasma discharge, cannot propagate through optical fiber, and typically returns a total electrical-to-optical power efficiency of 10–15%, all of which would hinder sampling applications in remote field locations. (Kennedy et al., 2004)

In the past quarter-century, the ytterbium (Yb)-doped fiber laser system has achieved more than a hundred-fold increase in maximum output power and consequently widespread adoption in communications, manufacturing, and defense. (Hecht, 2018) The use of highly-doped optical fiber as a gain medium—efficient to cool, tunable with Bragg gratings, and forming a long and high-gain cavity in a compact package—allows typical wall-plug efficiencies of over 30%. (Shi et al., 2014) The near-infrared (NIR) output wavelengths can be transmitted with extremely low loss by optical fiber. Further, their high reliability and output modulation allows one to machine materials with millisecond-range pulses or continuous wave (CW) radiation. A few groups have experimented with the use of this wavelength on ice—the aforementioned Sakurai et al. considered it before concluding that 10.6 µm was more worthy of experimentation, and Stone Aerospace Corp. has explored a direct borehole-drilling concept for interplanetary probes (Hogan et al., 2016) (Stone et al., 2019)—but none have progressed beyond laboratory testing. The primary drawback of the NIR is its absorption length in ice of ∼1 cm (Warren and Brandt, 2008) (Sakurai et al., 2016), which is much longer than the sub-millimeter distance over which 10.6 µm is absorbed. However, the efficiency, portability, and other advantages of doped fiber sources and the transmission abilities of optical fiber argue that the shorter wavelength cannot be dismissed. Indeed, Sakurai et al. also found that the drilling speed of a CO_2 laser is only about half the theoretical when meltwater is present, so a shorter absorption length may not be the incredible advantage that it initially appears.

Motivations

Many glaciological and paleoclimatological research methods measure ice characteristics that could potentially be disrupted by partial melting or water presence, such as chemical composition, crystal fabric, or trapped gas content (Tison, 1994) (Raynaud et al., 1982) (Mächler et al., 2023). While every mechanism for excising ice samples disrupts to some degree the ice immediately surrounding the cut, and it is standard practice for many techniques to remove the potentially contaminated or compromised outer layers (Osterberg et al., 2006) (Zdanowicz et al., 2016) (Winstrup et al., 2019), it is desirable to minimize the affected volume. Laser machining avoids physical cutters, and thus poses no risk of introducing metal shavings or other contaminant matter. The lack of toothed implements impacting or rubbing against portions of the sample also implies a significant reduction in externally-originated vibration and shock.

The overall feasibility of using a laser to excise a self-terminating triangular wedge from a mass of ice is easily demonstrated. In Fig. 1a—1c, a tap water ice cylinder 75 mm in diameter stands on a vertical linear motion stage which is in turn attached to a rotation stage, allowing a stationary Nd:YAG 1064 nm laser to trace a rectangular path 20 mm tall and spanning 90° of arc on the cylinder surface. After approximately 420 s of exposure to a 90 W CW beam, comprising just under 10 path traversals, the wedge of ice is completely freed and falls to the bottom of its slot. In Fig. 1d—1e, upgrading to a 1070 nm Yb-doped fiber laser allows the delivery optic to be maneuvered around a stationary ice target, as would be the case when retrieving samples from a borehole. 105 s of exposure to a 300 W CW beam, comprising three traversals of a closed path, cut free from a 50 mm ice cylinder a wedge approximately 30 mm tall and spanning 20° of arc. While these demonstrations easily achieve their goal of excising samples, the apparent internal clouding and bubble formation, kerf wider than 5 mm, and rapid surface heating all suggest a clear need to optimize laser cutting parameters.

The primary current impact of concern in a laser-based technique is thus the temperature rise of ice around the cut, or analogously, the radius around the cut which experiences a certain temperature increase. A widely used solution in industrial laser material processing is to use pulsed, instead of continuous-wave (CW), laser light, delivering a sufficient amount of thermal energy to melt or ablate a small volume with minimum heating. Removal of material is often assisted by the phenomena of melt ejection (Voisey et al., 2003), or artificially using pressurized gas (Majumdar and Manna, 2003). While ejection is unlikely to occur here due to the long NIR absorption length in ice reducing delivered power densities, and gas assistance on a borehole tool would incur additional mechanical complexity, the overall approach of pulsed lasers to limit widespread conduction may still be valid.

BACKGROUND AND METHODS

Our experiments use an IPG Photonics YLR-1000 Yb-doped fiber laser, producing a multi-mode beam of 1.07 µm wavelength which exits its delivery fiber through a collimator (IPG P30-001459) with a focal length of 50 mm. Pulsed and CW tests both use a 500 W nominal beam power, approximately half of the 1 kW stated capability of the source. A high-reflectivity 45° dielectric mirror (Thorlabs NB1-K13) transitions the beam from its initial downward vertical trajectory to horizontal, and two external lenses (Thorlabs LA1509-YAG and Newport KPC040AR.16) recollimate the beam to an approximately 1 mm spot over the ice sample's thickness. A silicon photodiode (Thorlabs FDS100) mounted behind the mirror and monitored by an oscilloscope (Tektronix TDS3014B) provides confirmation that the correct laser pulse parameters are delivered. To limit the number of variables at play, the laser pulses are shaped as an approximately-rectangular trapezoid: each increases linearly

from zero power to 500 W over 0.1 ms, maintains that power for the stated pulse time duration (e.g., 5 ms), and ramps back to zero power over 0.1 ms. An overview of the experiment setup is shown in Fig. 3a.

To enable profiling of the holes or cuts formed by laser exposure, samples of ice with relatively few bubbles or other visible-light scatterers were obtained by freezing lightly-filtered tap water in a silicone mold atop a larger foam-insulated water reservoir, the intent being to encourage directional freezing and bubble migration downward from the desired samples. (Wright et al., 2023) The mold is filled at room temperature and is placed in a -20 °C laboratory freezer for at least 48 hours, after which the resulting 5 cm cubes typically show bubbles and other near-surface features on four of their six faces, with the remaining two neighboring faces smooth and clear. Cubes were used at randomly-chosen orientations to minimize the possible impact of preferentially-oriented crystal structures, heat transfer rates, and other characteristics resulting from directional freezing. (Zhang et al., 2021) During testing, each ice cube is held in a 3D-printed nylon holder with a rigid support at the bottom and tension arms on three faces, all of which come no closer than 25 mm to the laser impingement point or line. A white LED (Cree XHP50A) weakly masked by a 3 mm slit illuminates from above the portion of the cube to be irradiated, while a visible light camera (IDS Imaging uEye UI336xCP-C, with Navitar Zoom 6000 lens) observes the side face parallel to the laser path via an infrared-transmitting mirror (Thorlabs FM203). The use of illumination normal to the observation direction approximates the approach of visible-light dark-field microscopy, increasing contrast by requiring that features scatter light toward the observer to be visible. (Gage, 1920) (More optical elements or space would be required to tightly restrict the spatial extent of illumination, but the existing configuration does tighten the visible depth of field in the images.) This arrangement is depicted in Fig. 3b. Video framerate recordings were used whenever possible, and in many cases show the various cut features and behaviors—e.g., movements or other characteristics which develop over time—with greater clarity than single images can convey; these original videos are available in a separately-published dataset. (Mah et al., 2023a)

The temperature of the irradiated face of an ice sample is monitored by a LWIR microbolometer camera (Seek Thermal IQ-AAA), mounted above the horizontal cutting laser beam path such that it can image the ice cube with no perspective distortion (i.e., other than any inherent to its optics) in the side-to-side direction profiled. The face of the cube spans 210 pixels horizontally, translating to a spatial resolution of 4.2 mm per pixel. Thermography pixel data, including corrections and "proprietary optimizations" by camera manufacturer Seek Thermal's application programming interface, is exported uncompressed. The laser impingement point, which can vary slightly between various experimental runs due to adjustments in the camera's vertical viewing angle, is located to the closest pixel as the maximum temperature seen in a 30 pixel tall parallelogram, and a line of pixels parallel to the bottom of the cube is vertically offset to pass through this maximum. An example thermal data frame, processed into a false color image, is shown in Fig. 7.

Observations on stationary drilling are not entirely descriptive of a sampling application, which would entail the cutting of straight or curved slots; these are likely to reduce the holding power of capillary forces on meltwater. The ice sample and white LED illumination source are therefore mounted on a stepper-powered linear motion stage (Befenybay SFU1605, driven by Copley Controls STP-075-07) which moves the sample up and down relative to the laser beam and observation equipment, enabling the laser to traverse a vertical strip across the entire height of the cube if desired. A set of graphite blocks (McMaster-Carr 9121K63/9121K65) is positioned 20 cm behind the sample to safely dissipate any laser energy not absorbed by the ice. All experiments are performed in a laboratory chest freezer (Scientemp 34-09A) maintaining a temperature of -17 °C ±3 °C.

RESULTS AND DISCUSSION

Stationary hole formation

To examine the initial interaction of ice with a 1070 nm laser, square pulses with durations between 1 and 50 ms were programmed into the IPG laser's internal controller (which has a time resolution of ±0.0036 ms) and applied at a repetition rate of 5 Hz, chosen for compatibility with a large range of pulse durations and good observability at video frame rates, for a total of 4 s. The power of each pulse was held at 500 W through the varying durations, yielding time-averaged powers ranging from 2.5 to 25 W. Visible-wavelength images show that each pulse causes a whitish conical profile to form along the beam's trajectory, fading quickly as the pulse ends. This conical edge advances more quickly through the ice for longer pulse durations, and makes negligible progress for pulses shorter than 2 ms. After a certain depth into the ice, the well-defined cone begins to be preceded and partly obscured by a looser cluster of strongly-scattering features. These resemble spherical bubbles and are observed to be highly mobile, suggesting that they are gas pockets forming in melted ice. Behind these leading edge effects, a sharp, approximately cylindrical outline denotes a tube of meltwater formed in the ice; this artifact is much longer lasting, lasting for sometimes minutes after the cessation of drilling, and often develops a downward bulge as the liquid expands the initially-symmetrical cavity. Initially the only water drainage seen—and only for pulse durations longer than about 10 ms—is a small bubble of air which extends a few millimeters into the cavity, likely due to capillary forces; if drilling is continued until the cavity front breaches the far side of the ice sample, more complete drainage is seen. An example of early drilling cavity progression is shown in Fig. 2.

Linear cut behaviors

Investigations of linear cuts were performed by moving the sample downward at 0.5 mm/s while applying laser pulses at 10 Hz. (Both rates were chosen to be easily observable at the frame rates of our visible-light camera and thermal cameras; faster speeds would be desirable in actual use, but these studies provide an indicator of behaviors with pulse lengths, repetition rates, and

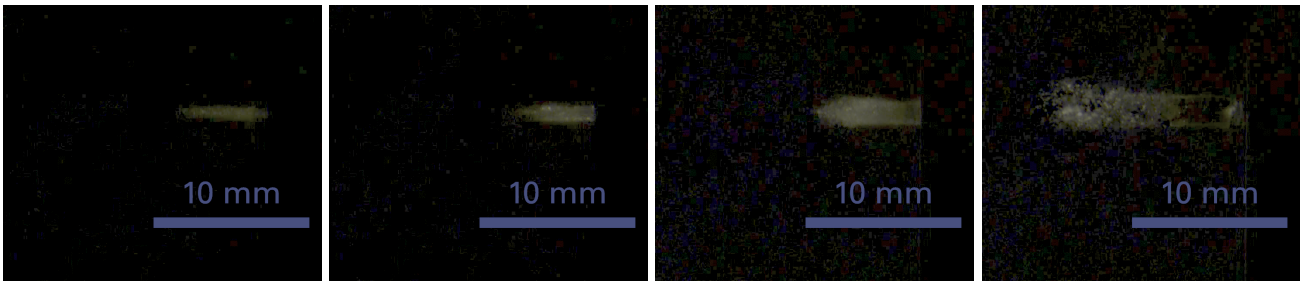

(a) After 1 pulse (b) 2 pulses (c) 7 pulses (d) 20 pulses

Fig. 2: The effects of (a) one, (b) two, (c) seven, and (d) twenty 12 ms 500 W square laser pulses on a tap-water ice cube. The pulses are delivered at 0.2 s intervals onto the face of a tap-water ice cube (the beam originating from the right side of the image, traveling towards the left) and the results recorded at ∼30 Hz from the side through approximately 7 mm of ice. A pre-laser image has been subtracted to reduce the visibility of preexisting features in the ice.

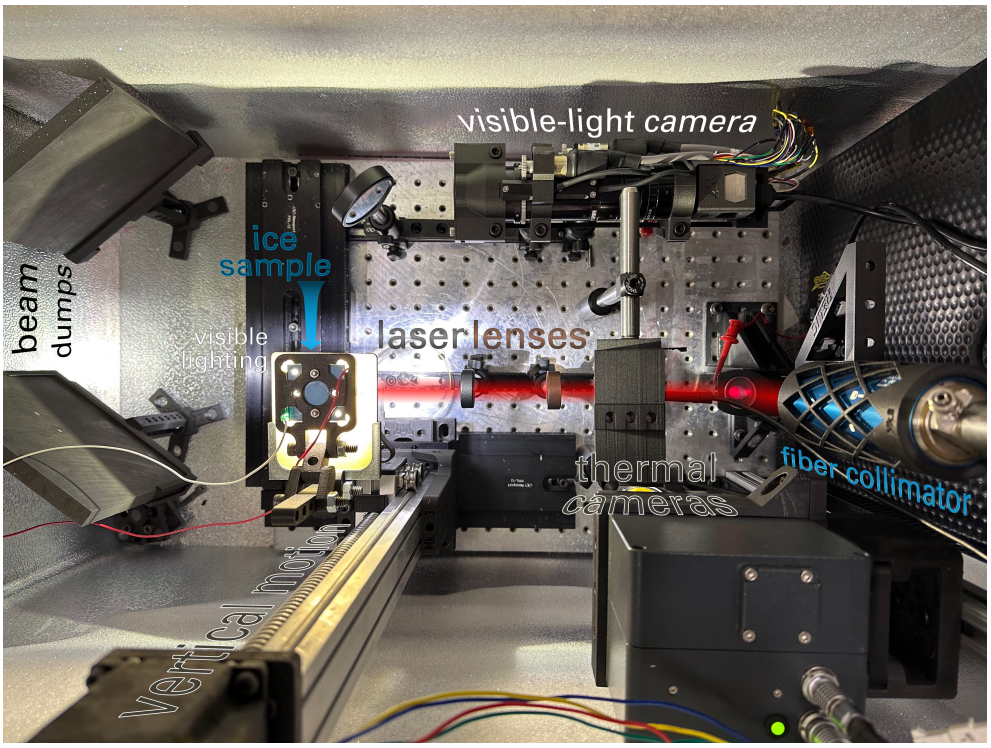

(a) Overhead view of experimental setup

Fig. 3: Images of equipment used to record ice behaviors during laser drilling and cutting. (a) A labeled overhead view of the experimental setup, installed within a laboratory chest freezer. The laser beam path has been depicted in red. *(figure continues on next page)*

sample movement speeds scaled up in synchrony.) Pulsing and movement were sustained for 50 s, resulting in the laser tracing a 25 mm strip on the face of the ice cube, beginning and ending a minimum of 5 mm away from the top and bottom edges. Visible-light imaging reveals that, for pulses longer than 2 ms, meltwater forms in the laser-irradiated region—as evidenced by air bubbles and other scattering features moving around and predominantly upwards—and drains out of the entrance once the laser spot has traveled a certain distance upwards, revealing an air-filled slot in the ice. (Droplets of refrozen meltwater are usually found on the sample mounts, supporting structures, or sometimes on the bottom face of the ice cube.) The maximum depth and the shape of the slot varies with pulse duration: 5 ms pulses reliably produce a rectangular shape with rounded inner corners, while 9 ms pulses produce a highly irregular cavity with conical-appearing protrusions traveling farther and slightly upwards into the cube. Other light-scattering features were also observed to form in the ice surrounding the air-filled slot, consistent with those observed in hole drilling, and their visibility again increases quickly with pulse duration, such that a cavity formed by 5 ms pulses will generally have only a smattering of small scattering centers beyond its borders but a slot cut by 10 ms pulses will be surrounded and partially obscured by a cloud of scatterers. Measurements with a ruler approx. 30 s

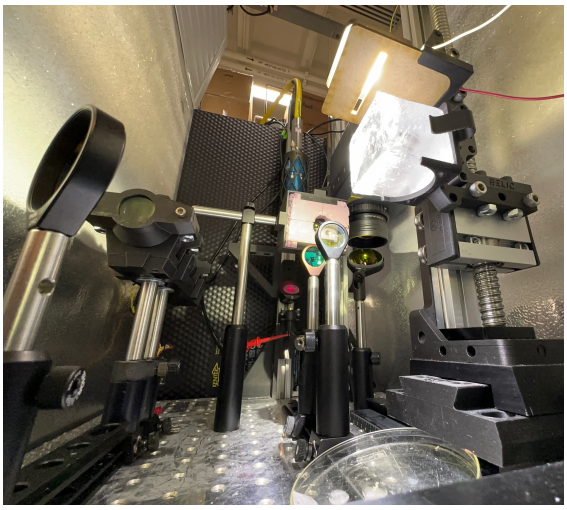

(b) Visible-light sample illumination and imaging

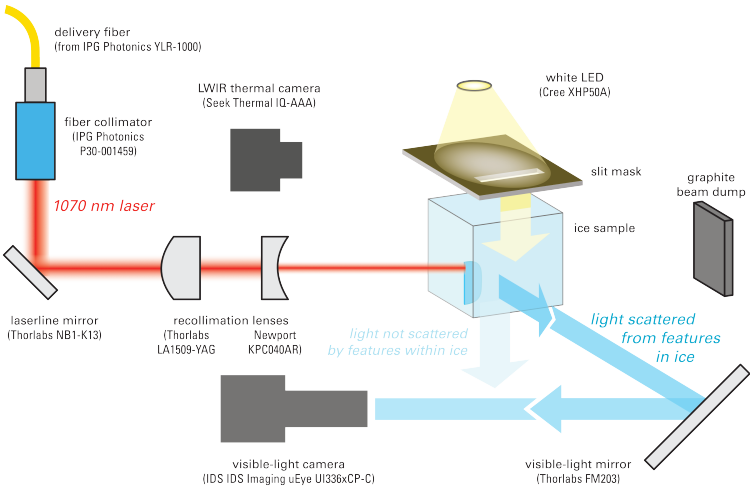

(c) Block diagram

Fig. 3: *(continued from previous page)* (b) Looking back and upwards towards the setup from the beam dumps. The ice sample, seen here in a raised position for loading, is illuminated by a white light-emitting diode positioned just above a 0.3 mm wide slit to loosely limit its spatial extent. At image left, the visible-light camera views the sample's side face—and thus the depth profile of laser-formed holes or slots, via perpendicularly-refracted light—through an IR-transmitting cold mirror both to address space constraints and to help prevent NIR laser light from damaging the sensor. Near image center, the thermal imaging camera is housed in a pink foam insulated casing and mounted over the cutting beam path to minimize distortion lateral to sample movement. (c) A block diagram of the optical setup, drawn neither to scale nor perspective.

after laser cessation find the slot between 1.0 and 1.5 mm wide at the cube's surface, with sharply-defined edges regardless of pulse duration. Example images are shown in Fig. 4.

We define the maximum depth of the slot to be the distance, parallel to the image top and bottom edges, from the irradiated face of the cube to the farthest visually-identified boundary of the air-filled cavity. Plotting this quantity versus pulse duration in Fig. 5 reveals a highly linear relationship (depth $= 3.328 \cdot t_{\text{pulse}} - 6.485$, $R^2 = 0.996$) throughout the test range, up to approximately 34 mm for 12 ms pulses. This is expected, as the duration of the square pulses are directly proportional to the total amount of energy per time delivered to the ice, and confirms that a constant portion of the energy is being directly translated into cutting progress.

Thermal impacts

In order to isolate the impact of pulse duration on cut slot formation, the total number of pulses delivered in a fixed amount of time must change inversely to duration of each pulse in order to hold constant the overall energy delivered; otherwise, any observed effects may be a result of a different total heat input rather than its distribution in time. A series of such cutting tests was executed with time-averaged power held constant at 25.5 W, equivalent to 10x 5 ms pulses. The resulting maximum slot depths are plotted in Fig. 6. A loose linear fit (depth $= -0.038 \cdot t_{\text{pulse}} + 0.727$, $R^2 = 0.441$) suggests that shorter laser pulses deliver a larger maximum slot depth. CW cutting, essentially equivalent to a pulse duration of 100 ms, defies comparison using this measurement method both by causing internal clouding severe enough to entirely conceal the slot profile and by penetrating the entire 5 cm thickness of the ice sample.

Thermal images were taken concurrently with the visible-light observations of static hole drilling, and temperatures were extracted along a profile line passing through the laser impingement point and parallel with the bottom edge of the cube. This temperature data, an example of which is displayed in Fig. 7, shows an exponential rise towards the laser impingement point. As the amount of heating that would compromise scientific value varies by the ice characteristic to be measured, we use as a metric the half-width half-maximum (HWHM) heating distance, which we define as the length needed for the temperature to drop halfway from the maximum seen at the laser impingement point. This maximum temperature may reflect the meltwater and hole viewing angle more than the actual temperature of the surrounding ice, so we fix the maximum temperature at 0 °C. The extent of heated ice thus defined, as shown in Fig. 8a, ranges from 0.7 mm for 3 ms pulses to 2.4 mm for 50 ms durations. (Pulses shorter than 3 ms did not exhibit temperatures above 0 °C at the laser impingement point.) These distances follow an approximately linear growth (HWHM $= 0.0285 \cdot t_{\text{pulse}} + 0.948$, $R^2 = 0.761$) according to pulse duration. In contrast, a 4 s CW irradiation resulted in a HWHM of about 16 mm, with detectable heating at the far edge of the ice sample.

A few other metrics of heating are plotted in Fig. 8b. The temperature (averaged over about 10 pixels, or 2.35 mm) at the ice edge farthest from the irradiation point is effectively constant versus pulse durations, indicating no measurable heating has spread to the far edge of the ice; a sample being excised from an ice sheet would be in contact, albeit with decreasing

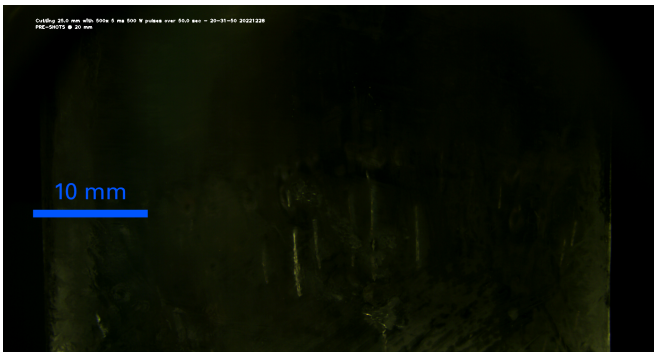

(a) Before 5 ms pulses

(b) Before 9 ms pulses

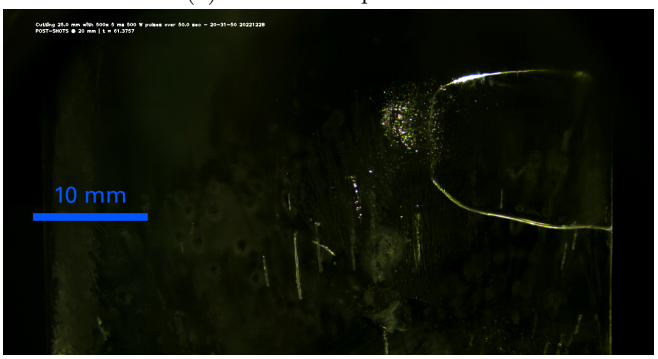

(c) After 5 ms pulses

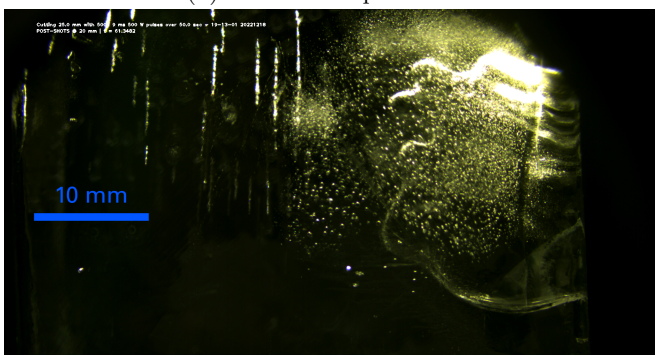

(d) After 9 ms pulses

(e) Difference before vs. after 5 ms pulses, annotated

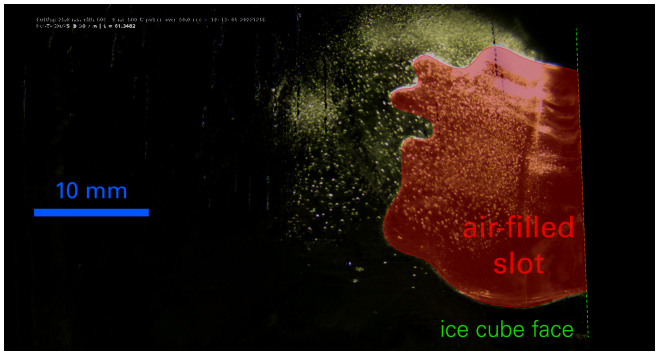

(f) Difference before vs. after 9 ms pulses, annotated

Fig. 4: Visible-light images of the side of tap-water ice cubes, before (top row) and after (middle row) the cutting of a self-evacuated slot by 500 total laser pulses of duration (left column) 5 ms and (right column) 9 ms square pulses over 50 s, during which the sample was moved downward at 0.5 mm/s. Images (a) and (b) were taken approximately 10 s before the onset of irradiation, while (c) and (d) were taken approximately 12 s after cessation of laser pulses. The bottom row of (e) and (f) are constructed by pixel-subtracting the respective pre-shot frames from their post-shot counterparts, and manually adding annotations. Note that the shorter laser pulses of the left column have produced a small patch of scattering features just beyond the slot's far border, while the longer pulses have produced a much larger and denser cloud of light scatterers of varying sizes.

area, to an effectively infinite heat sink, so keeping the total laser sequence brief allows us to ignore this stark difference in boundary conditions. At the opposite end of the stability spectrum is the temperature seen at the hottest, laser impingement point, which displays a mostly-linear trend and individual variations heavily reminiscent of the HWHM distance, suggesting that the rest of the temperature profile does follow the maximum observed point's variations and that they are not, as we had feared, simply artifacts of laser exposure. Finally, the temperature 2.35 mm away from the laser spot shows a slower but still reasonably linear growth, reinforcing the HWHM finding.

Discussion and next steps

We now have evidence that pulse duration (>3 ms) relates roughly linearly to both the slot depth in cutting, at approximately 3.33 mm per pulse ms, and the radius of warned ice when drilling, at about 0.0285 mm per pulse ms. Simple extrapolation of

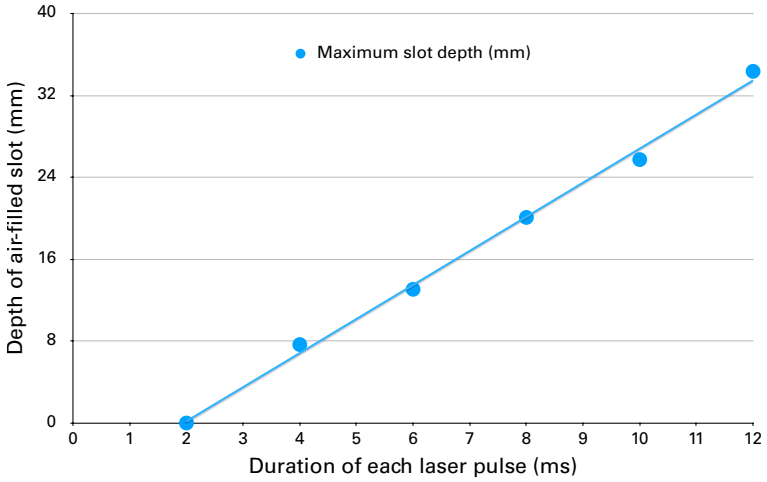

Fig. 5: Plot of maximum depth of an air-filled slot versus the duration of laser pulse used to form it.

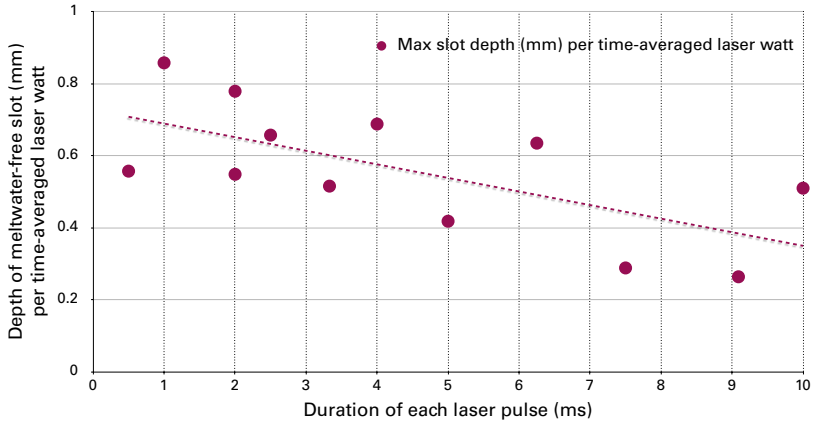

Fig. 6: Plot of maximum depth of an air-filled slot formed by laser pulses of varying duration, repetition rate, and total number adjusted to maintain a constant time-averaged energy input rate into the ice sample. (Each observed depth value is divided by an energy calculated to include the 0.1 ms ramp-up and -down period on each otherwise square pulse, which grows more significant with shorter pulses.)

these two linear fits imply that a laser cutting system could gain 117 mm of slot depth per additional radial mm of warmed ice. At our chosen cutting speed of at 0.5 mm/s, the ∼1 mm laser spot will take a total of 2 s to traverse a given point on the ice and deliver to it 20 pulses, which is the same amount of energy we used in static drilling; however, our drilling measurements (which had to accommodate a low thermal camera frame rate) spread this dose out over 4 s, and the >1 mm HWHM for pulses above 5 ms suggests that significant temperature influence continued for a second or two after the slot-cutting laser has moved away. Nevertheless, these results suggest that a laser-excised sample could easily keep all but 2 mm of ice on each face from having experienced a rise of more than 10 °C even with a fairly aggressive cutting rate, 50 ms pulses at 10 Hz being equal to a 50% duty cycle.

These experiments represent a necessary first step in the characterization of ice behavior under NIR laser cutting, but many aspects remain to be investigated. The directionally-frozen tap water ice samples used here were chosen for their relative visual clarity to enable cut profile observations and their simple preparation to supply a consumptive testing campaign; they are likely to have anisotropic mechanical structure (although we did not note any obvious asymmetries in our drilling and cutting observations or thermal measurements), higher electrolytic conductivity (Gow, 1968), and almost certainly depart in other ways from the characteristics—highly varied as they are—of natural glacier ice, which should be tested as optimization continues in subsequent experiments. Thermal imaging measures immediate temperatures on the surface of the ice, but not farther into the sample's bulk, as the LWIR wavelengths used have a very short absorption length; since thermal conduction through solid ice will dissipate heat much more effectively than the interface between ice and air, and the laser beam is decreasing in irradiance as it refracts, absorbs, and scatters deeper into the ice, this surface temperature reading will represent the maximum. Flowing meltwater removes heat from the area it is departing, and therefore thermal readings on stationary drilled holes are likely overestimates of temperature during cutting. The most concerning phenomenon observed is the light-scattering features which

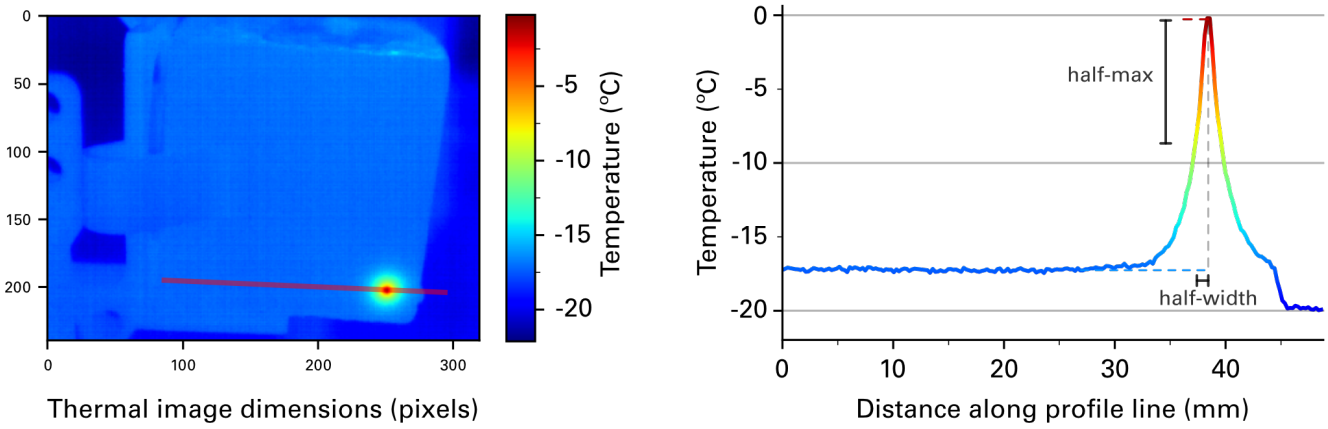

(a) Image

(b) Temperature profile

Fig. 7: Excerpts from the processing of one example thermal image. (a) The thermography data supplied by the camera, an uncompressed floating-point temperature array, visualized in a false-color image. The red semitransparent line near the bottom of the frame indicates the one-dimensional slice along which we will profile the ice surface temperatures. (b) The temperature along said profile line, with the half-width half-maximum heating distance indicated in blue. Note that the maximum is taken to be 0 °C to prevent factors such as hole depth and pulse timing from artificially reducing the HWHM, and that we ignore all data to the right of the laser peak, as the ice sample quickly gives way to the freezer background. The dashed horizontal line near -17 °C denotes the initial temperature of the cube before any laser drilling.

were observed to form beyond and around an advancing hole or slot; while their exact nature warrants closer examination, these results suggest that it is both possible and desirable to minimize their formation (and promote a neater, more rectangular slot profile) through the selection of laser pulses shorter than 10 ms, with cutting depth progress maintained by increasing repetition rate. Multiple cutting passes can be used, as further irradiation of a previously-cut cavity or slot without standing water should be effectively the same (except for the added propagation distance in air) as the initial cut on the original surface. Finally, a square pulse of varying width is only the simplest form of modulation possible with a modern fiber laser. More complex or varying pulse shapes, dynamic repetition rates, beam focusing instead of collimation to limit the irradiated depth of ice, and faster travel speeds are all parameters which may offer process optimizations upon systematic examination.

CONCLUSIONS

Sequences of millisecond-regime 500 W pulses of 1070 nm laser light have been demonstrated to easily and effectively cut tap-water ice samples, producing a linear vertical slot which promotes rapid self-evacuation of meltwater. The maximum slot depth increases in direct proportion with the duration of each square laser pulse in the 500-pulse 10 Hz sequence used to produce it, at up to 34 mm for 12 ms pulses. In stationary drilling experiments with 20-pulse 5 Hz sequences, representing the worst case of meltwater remaining in a cut, the radius of ice that rises halfway to melting from an initial temperature of -17 °C ±1 °C varies from 0.7 mm for a 3 ms pulse to 2.4 mm for a 50 ms pulse, with an approximately linear relationship. Simple extrapolation of these two linear trends imply that a laser cutting system could gain 117 mm of slot depth per additional radial mm of heat-compromised ice; however, as pulses lengthen to 10 ms, effects such as a tendency to irregular depth profiles and heavy concentrations of scattering centers nearby indicate that this simple scalability would quickly prove undesirable for delicate samples. Tests maintaining a constant time-averaged power suggest that for the simple pulse shape tested, shorter—e.g., below 10 ms—pulses and attendant higher repetition rates are preferable to longer, slower pulses for producing clean cuts and minimizing heating.

ACKNOWLEDGEMENTS

This work was supported by U.S. National Science Foundation grants 2032463 and 2032473. Acquisition of the laser source and associated equipment was jointly funded by the NSF and the Joint Directed Energy Transition Office / Office of Naval Research, the latter under grant N00014-17-1-2438. Rapid-prototyped sample holders and other mechanical parts were made possible by the resources of the Anderson Student Innovation Labs, and the expert assistance therein of staff members Ben Guengerich and Ethan Polcyn.

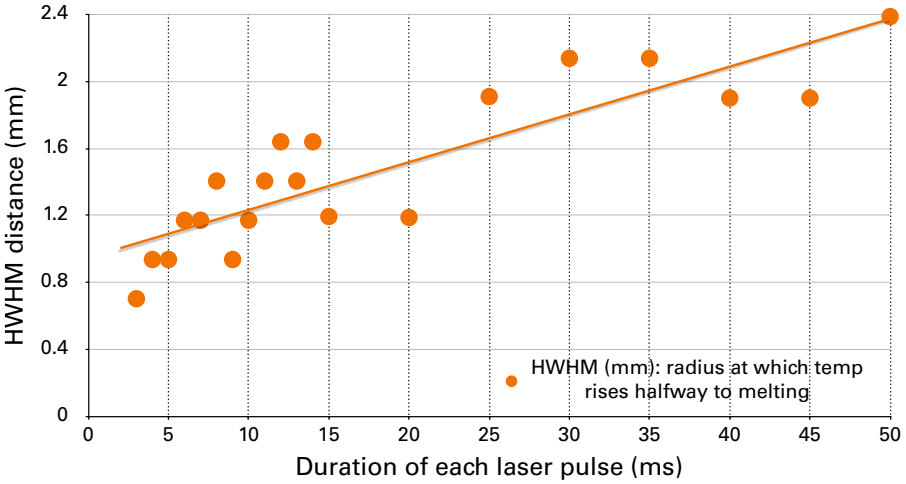

(a) Half-width half-maximum

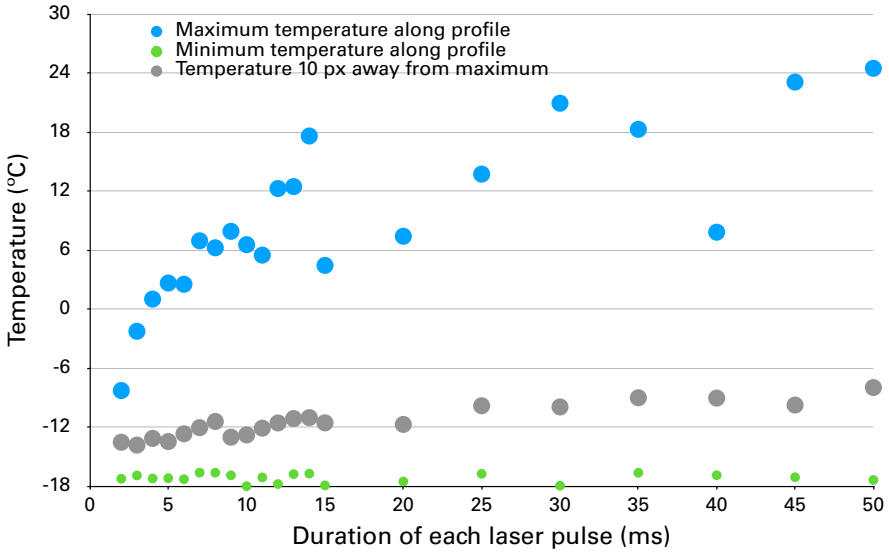

(b) Other heating metrics

Fig. 8: Several expressions of the peripheral heating versus the duration of a square laser pulse: (a) the half-width half-maximum heating distance, taken as the maximum seen over the 4 s laser shot sequence, and (b) the maximum (i.e., at the laser impingement spot), minimum, and 2.35 mm-from-impingent temperatures measured along the profile line in the first frame captured after the end of the shot sequence.

DATA AVAILABILITY

The raw data required to reproduce the above findings are available to download from the U.S. Antarctic Program Data Center repository, hosted at Lamont-Doherty Earth Observatory of Columbia University: `https://www.usap-dc.org/view/dataset/601753`. (Mah et al., 2023a) The same dataset is also available at Zenodo: `https://zenodo.org/records/13575104`. (Mah et al., 2023b)

REFERENCES

Ahn J, Wahlen M, Deck BL, Brook EJ, Mayewski PA, Taylor KC and White JWC (2004) A record of atmospheric CO2 during the last 40,000 years from the Siple Dome, Antarctica ice core. *Journal of Geophysical Research: Atmospheres*, **109**(D13), ISSN 2156-2202 (doi: 10.1029/2003JD004415)

Bohleber P, Roman M, Šala M and Barbante C (2020) Imaging the impurity distribution in glacier ice cores with LA-ICP-MS. *Journal of Analytical Atomic Spectrometry*, **35**(10), 2204–2212 (doi: 10.1039/D0JA00170H)

Cheng J, Liu Cs, Shang S, Liu D, Perrie W, Dearden G and Watkins K (2013) A review of ultrafast laser materials micromachining. *Optics & Laser Technology*, **46**, 88–102, ISSN 0030-3992 (doi: 10.1016/j.optlastec.2012.06.037)

Chichkov BN, Momma C, Nolte S, von Alvensleben F and Tünnermann A (1996) Femtosecond, picosecond and nanosecond laser ablation of solids. *Applied Physics A*, **63**(2), 109–115, ISSN 1432-0630 (doi: 10.1007/BF01567637)

Clark AF, Moulder JC and Reed RP (1973) Ability of a CO2 laser to assist ice breakers. *Applied Optics*, **12**(6), 1103–1104, ISSN 2155-3165 (doi: 10.1364/AO.12.001103)

Davidge L, Brooks HL and Mah ML (2022) From drilling to data: Retrieval, transportation, analysis, and long-term storage of ice-core samples. *Past Global Changes Magazine*, **30**(2), 98–99, ISSN 2411605X, 24119180

Eshelman EJ, Malaska MJ, Manatt KS, Doloboff IJ, Wanger G, Willis MC, Abbey WJ, Beegle LW, Priscu JC and Bhartia R (2019) WATSON: *In Situ* organic detection in subsurface ice using deep-UV fluorescence spectroscopy. *Astrobiology*, **19**(6), 771–784, ISSN 1531-1074, 1557-8070 (doi: 10.1089/ast.2018.1925)

Gage SH (1920) Modern dark-field microscopy and the history of its development. *Transactions of the American Microscopical Society*, **39**(2), 95–141, ISSN 0003-0023 (doi: 10.2307/3221838)

Goodge JW and Severinghaus JP (2016) Rapid Access Ice Drill: A new tool for exploration of the deep Antarctic ice sheets and subglacial geology. *Journal of Glaciology*, **62**(236), 1049–1064, ISSN 0022-1430, 1727-5652 (doi: 10.1017/jog.2016.97)

Gow AJ (1968) Electrolytic conductivity of snow and glacier ice from Antarctica and Greenland. *Journal of Geophysical Research (1896-1977)*, **73**(12), 3643–3649, ISSN 2156-2202 (doi: 10.1029/JB073i012p03643)

Gow AJ and Meese D (2007) Physical properties, crystalline textures and c-axis fabrics of the Siple Dome (Antarctica) ice core. *Journal of Glaciology*, **53**(183), 573–584 (doi: 10.3189/002214307784409252)

Hecht J (2018) High-Power Fiber Lasers. *Optics and Photonics News*, **29**(10), 30–37, ISSN 1541-3721

Hogan B, Stone W, Bramall NE, Siegel V, Lelievre S, Rothhammer B, Richmond K and Flesher C (2016) Direct laser ice penetrator for exploring icy ocean worlds: Design, modeling and test results of a proof-of-concept prototype. In *AGU Fall Meeting 2016*, volume 2016, C53B–0708, American Geophysical Union

Kennedy E, Byrne G and Collins DN (2004) A review of the use of high power diode lasers in surface hardening. *Journal of Materials Processing Technology*, **155–156**, 1855–1860, ISSN 0924-0136 (doi: 10.1016/j.jmatprotec.2004.04.276)

Lunga DD, Müller W, Rasmussen SO and Svensson A (2014) Location of cation impurities in NGRIP deep ice revealed by cryo-cell UV-laser-ablation ICPMS. *Journal of Glaciology*, **60**(223), 970–988, ISSN 0022-1430, 1727-5652 (doi: 10.3189/2014JoG13J199)

Mächler L, Baggenstos D, Krauss F, Schmitt J, Bereiter B, Walther R, Reinhard C, Tuzson B, Emmenegger L and Fischer H (2023) Laser-induced sublimation extraction for centimeter-resolution multi-species greenhouse gas analysis on ice cores. *Atmospheric Measurement Techniques*, **16**(2), 355–372, ISSN 1867-8548 (doi: 10.5194/amt-16-355-2023)

Mah M, Kurbatov AV and Talghader JJ (2023a) Visual, thermal, chemical, and stable isotope effects of near-infrared laser cutting on freezer ice. U.S. Antarctic Program (USAP) Data Center. `https://www.usap-dc.org/view/dataset/601753` (doi: 10.15784/601753)

Mah M, Kurbatov AV and Talghader JJ (2023b) Visual, thermal, chemical, and stable isotope effects of near-infrared laser cutting on freezer ice. Zenodo. `https://zenodo.org/records/13575104` (doi: 10.15784/601753)

Majumdar JD and Manna I (2003) Laser processing of materials. *Sadhana*, **28**(3-4), 495–562

Müller W, Shelley JMG and Rasmussen SO (2011) Direct chemical analysis of frozen ice cores by UV-laser ablation ICPMS. *Journal of Analytical Atomic Spectrometry*, **26**(12), 2391–2395, ISSN 1364-5544 (doi: 10.1039/C1JA10242G)

Osterberg EC, Handley MJ, Sneed SB, Mayewski PA and Kreutz KJ (2006) Continuous ice core melter system with discrete sampling for major ion, trace element, and stable isotope analyses. *Environmental Science & Technology*, **40**(10), 3355–3361, ISSN 0013-936X (doi: 10.1021/es052536w)

Peensoo KM (2021) *Developing a Method for High Resolution Water Isotope Measurements in Ice Cores*. Master's thesis, University of Copenhagen

Raynaud D, Delmas R, Ascencio JM and Legrand M (1982) Gas extraction from polar ice cores: A critical issue for studying the evolution of atmospheric CO2 and ice-sheet surface elevation. *Annals of Glaciology*, **3**, 265–268, ISSN 0260-3055, 1727-5644 (doi: 10.3189/S0260305500002895)

Sakurai T, Chosrowjan H, Somekawa T, Fujita M, Motoyama H, Watanabe O and Izawa Y (2016) Studies of melting ice using CO2 laser for ice drilling. *Cold Regions Science and Technology*, **121**, 11–15, ISSN 0165-232X (doi: 10.1016/j.coldregions.2015.09.014)

Shi W, Fang Q, Zhu X, Norwood RA and Peyghambarian N (2014) Fiber lasers and their applications [Invited]. *Applied Optics*, **53**(28), 6554–6568, ISSN 2155-3165 (doi: 10.1364/AO.53.006554)

Slawny KR, Johnson JA, Mortensen NB, Gibson CJ, Goetz JJ, Shturmakov AJ, Lebar DA and Wendricks AW (2014) Production drilling at WAIS Divide. *Annals of Glaciology*, **55**(68), 147–155, ISSN 0260-3055, 1727-5644 (doi: 10.3189/2014AoG68A018)

Sneed SB, Mayewski PA, Sayre W, Handley MJ, Kurbatov AV, Taylor KC, Bohleber P, Wagenbach D, Erhardt T and Spaulding NE (2015) New LA-ICP-MS cryocell and calibration technique for sub-millimeter analysis of ice cores. *Journal of Glaciology*, **61**(226), 233–242, ISSN 00221430, 17275652 (doi: 10.3189/2015JoG14J139)

Stone W, Hogan B, Richmond K, Siegel VL, Lelievre S, Smith J, Flesher C, Moor J and Lopez A (2019) Environmental test results for a direct laser cryobot for ocean world missions. In *AGU Fall Meeting 2019*, volume 2019, P53E–3503, American Geophysical Union

Tison JL (1994) Instruments and Methods: Diamond wire-saw cutting technique for investigating textures and fabrics of debris-laden ice and brittle ice. *Journal of Glaciology*, **40**(135), 410–414, ISSN 0022-1430, 1727-5652 (doi: 10.3189/S0022143000007498)

Voisey KT, Kudesia SS, Rodden WSO, Hand DP, Jones JDC and Clyne TW (2003) Melt ejection during laser drilling of metals. *Materials Science and Engineering: A*, **356**(1), 414–424, ISSN 0921-5093 (doi: 10.1016/S0921-5093(03)00155-2)

Warren SG (2019) Optical properties of ice and snow. *Philosophical Transactions of the Royal Society A: Mathematical, Physical and Engineering Sciences*, **377**(2146), 20180161 (doi: 10.1098/rsta.2018.0161)

Warren SG and Brandt RE (2008) Optical constants of ice from the ultraviolet to the microwave: A revised compilation. *Journal of Geophysical Research: Atmospheres*, **113**(D14), D14220, ISSN 2156-2202 (doi: 10.1029/2007JD009744)

Winstrup M, Vallelonga P, Kjær HA, Fudge TJ, Lee JE, Riis MH, Edwards R, Bertler NAN, Blunier T, Brook EJ, Buizert C, Ciobanu G, Conway H, Dahl-Jensen D, Ellis A, Emanuelsson BD, Hindmarsh RCA, Keller ED, Kurbatov AV, Mayewski PA, Neff PD, Pyne RL, Simonsen MF, Svensson A, Tuohy A, Waddington ED and Wheatley S (2019) A 2700-year annual timescale and accumulation history for an ice core from Roosevelt Island, West Antarctica. *Climate of the Past*, **15**(2), 751–779, ISSN 1814-9324 (doi: 10.5194/cp-15-751-2019)

Wright KS, Awerkamp PA, Hill D, Bashaw B, Van Woerkom D, Fish D, Nordin GP and Camacho RM (2023) Freezing optically clear microdroplets in a laboratory setting. In *2023 Intermountain Engineering, Technology and Computing (IETC)*, 98–101 (doi: 10.1109/IETC57902.2023.10152156)

Zdanowicz CM, Krümmel EM, Poulain AJ, Yumvihoze E, Chen J, Štrok M, Scheer M and Hintelmann H (2016) Historical variations of mercury stable isotope ratios in Arctic glacier firn and ice cores. *Global Biogeochemical Cycles*, **30**(9), 1324–1347, ISSN 1944-9224 (doi: 10.1002/2016GB005411)

Zeller E, Dreschhoff G and Laird CM (1991) Development of laser ice-cutting apparatus. *Antarctic Journal of the United States*, **26**(5), 89–91

Zhang T, Wang L, Wang Z, Li J and Wang J (2021) Single ice crystal growth with controlled orientation during directional freezing. *The Journal of Physical Chemistry B*, **125**(3), 970–979, ISSN 1520-6106 (doi: 10.1021/acs.jpcb.0c11028)